

Photon Berry phases, Instantons, Schrodinger Cats with oscillating parities and crossover from $U(1)$ to Z_2 limit in cavity QED systems

Yu Yi-Xiang^{1,2,3}, Jinwu Ye^{1,3}, W.M. Liu² and CunLin Zhang³

¹ *Department of Physics and Astronomy, Mississippi State University, P. O. Box 5167, Mississippi State, MS, 39762*

² *Beijing National Laboratory for Condensed Matter Physics, Institute of Physics, Chinese Academy of Sciences, Beijing 100190, China*

³ *Key Laboratory of Terahertz Optoelectronics, Ministry of Education, Department of Physics, Capital Normal University, Beijing 100048, China*

(Dated: November 6, 2018)

The four standard quantum optics models such as Rabi, Dicke, Jaynes-Cummings (JC) and Tavis-Cummings (TC) model were proposed by the old generation of great physicists many decades ago. Despite their relative simple forms and many previous theoretical works, their solutions at a finite N , especially inside the superradiant regime, remain unknown. In this work, we address this outstanding problem by using the $1/J$ expansion and exact diagonalization to study the $U(1)/Z_2$ Dicke model at a finite N . This model includes the four standard quantum optics model as its various special limits. The $1/J$ expansions is complementary to the strong coupling expansion used by the authors in arXiv:1512.08581 to study the same model in its dual $Z_2/U(1)$ representation. We identify 3 regimes of the system's energy levels: the normal, $U(1)$ and quantum tunneling (QT) regime. The system's energy levels are grouped into doublets which consist of scattering states and Schrodinger Cats with even (e) and odd (o) parities in the $U(1)$ and quantum tunneling (QT) regime respectively. In the QT regime, by the WKB method, we find the emergencies of bound states one by one as the interaction strength increases, then investigate a new class of quantum tunneling processes through the instantons between the two bound states in the compact photon phase. It is the Berry phase interference effects in the instanton tunneling event which leads to Schrodinger Cats oscillating with even and odd parities in both ground and higher energy bound states. We map out the energy level evolution from the $U(1)$ to the QT regime and also discuss some duality relations between the energy levels in the two regimes. We also compute the photon correlation functions, squeezing spectrum, number correlation functions in both regimes which can be measured by various experimental techniques. The combinations of the results achieved here by $1/J$ expansion and those in arXiv:1512.08581 by strong coupling method lead to rather complete understandings of the $U(1)/Z_2$ Dicke model at a finite N and any anisotropy parameter β . Experimental realizations and detections are presented. Connections with past works and future perspectives are also discussed.

I. INTRODUCTION

Quantum optics is a subject to describe the atom-photon interactions^{1,2}. The history of quantum optics can be best followed by looking at the evolution of quantum optics models to study such interactions. In the Rabi model³, a single mode photon interacts with a two level atom with equal rotating wave (RW) and counter rotating wave (CRW) strength. To study possible many body effects such as "optical bombs", a single two level atoms in the Rabi model was extended to an assembly of N two level atoms in the Dicke model⁵. When the coupling strength is well below the transition frequency, the CRW term in the Rabi model is effectively much smaller than that of RW, so it was dropped in the Jaynes-Cummings (JC) model⁴. Similar to the generalization from the Rabi to the Dicke model, the single two level atom in the JC model was extended to an assembly of N two level atoms in the Tavis-Cummings (TC) model⁶.

The importance of the 4 standard quantum optics model at a finite N in quantum and non-linear optics ranks the same as the bosonic or fermionic Hubbard models and Heisenberg models in strongly correlated electron systems and the Ising models in Statistical mechanics^{7,8}. There have been extensive theoretical investigations on

the solutions of the four standard quantum optics model. Most of the theoretical works focused on the thermodynamic limit $N \rightarrow \infty$. The TC model was studied at $N \rightarrow \infty$ in⁹⁻¹². A normal to a superradiant phase transition was found and the zero mode due to the broken $U(1)$ symmetry identified in the superradiant phase. The Dicke model at $N \rightarrow \infty$ was investigated in¹³. A superradiant phase transition with the broken Z_2 symmetry was found and two gapped modes due to the broken Z_2 symmetry identified in the superradiant phase. However, there were only very limited works at a finite N . The Exact Diagonalization (ED) in¹³ shows that the level statistics in a give parity sector changes from the Poissonian distribution in the normal phase to the Wigner-Dyson in the superradiant phase at any finite N . For the Dicke model, the ground state photon number at the normal to the superradiant quantum critical point QCP was found^{14,15} to scale as $\langle n_{ph} \rangle \sim cN^{1/3}$ which is a direct consequence of finite size scaling near a QCP with infinite coordination numbers^{16,17}. There are also formally "exact" Bethe Ansatz-like solution for the integrable TC model at a finite N ¹⁸. Recently, a formal "exact" solution was found even for the non-integrable Dicke model at $N = 1$ (Rabi model)¹⁹. Unfortunately, these "exact" solutions are essentially useless in extracting any physical

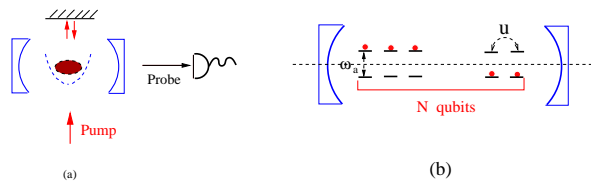


FIG. 1. (a) Cold or thermal atoms in a trap embedded in a cavity in the strong coupling regime with a transverse pumping^{27–29}. The probe detects the Fluorescence spectrum of the cavity leaking photons. (b) $N = 2 \sim 9$ superconducting qubits are placed on the one or more anti-nodes of a circuit QED resonator^{30–34}.

phenomena^{18,19}.

It is convenient to classify the four well known quantum optics models from a simple symmetry point of view: the TC and Dicke model as $U(1)$ and Z_2 Dicke model respectively, while JC and Rabi model are just as the $N = 1$ version of the two^{20–22}. In fact, as stressed in²¹, there are also two different representations on all of the 4 models: N – representation with N independent two level atoms with a large Hilbert space 2^N and spin $J = N/2$ representation with a smaller Hilbert space $N + 1$. The relations between the two representations were clarified in²¹. The dramatic finite size effects such as the Berry phase effects, Goldstone and Higgs modes on $U(1)$ Dicke model were thoroughly discussed in both N – representation in²⁰ by $1/N$ expansion and spin- $J = N/2$ representation²¹ by $1/J$ representation. Remarkably, we find nearly perfect agreements between the results achieved by $1/N$ and $1/J$ and the ED studies even when N gets to its lowest value $N = 1$. The effects of a small CRW term near the $U(1)$ Dicke model limit was also studied in²¹. In view of the tremendous success of the $1/N$ and $1/J$ expansion in studying many strongly correlated electron systems^{23,24}, particularly in the $U(1)$ Dicke model achieved in^{20–22}, it is natural to apply them to study the Z_2 Dicke model as originally planned in²⁰.

Due to recent tremendous advances in technologies, the 4 standard quantum optics models were successfully achieved in at least two experimental systems (1) with a BEC of $N \sim 10^5$ ⁸⁷Rb atoms inside an ultrahigh-finesse optical cavity^{25–29} and (2) superconducting qubits inside a microwave circuit cavity^{30–33} or quantum dots inside a semi-conductor microcavity³⁴. The superradiant phase in the Dicke model was also realized in system (1) with the help of transverse pumping (Fig.1a)^{27–29}. It could also be realized "spontaneously" in the system (2) without external pumping²¹. Indeed, by enhancing the inductive coupling of a flux qubit to a transmission line resonator, a remarkable ultra-strong coupling with individual $\tilde{g} \sim 0.12\omega_a$ was realized in a circuit QED system³³. However, in such a ultra-strong coupling regime, the system is described well neither by the TC model nor the Dicke model, but a combination of the two Eqn.1 with unequal RW and CRW strength dubbed as $U(1)/Z_2$ Dicke model in²¹. It was also proposed in³⁵ that in the

thermal or cold atom experiments, the strengths of g and g' can be tuned separately by using circularly polarized pump beams in a ring cavity. Indeed, based on the scheme, a recent experiment³⁶ realized the $U(1)/Z_2$ Dicke model with continuously tunable g and g' . As argued in^{20,21}, with only a few $N = 2 \sim 9$ qubits embedded in system (2), the finite size effects may become important and experimentally observable. With the recent advances of manipulating a few to a few hundreds of cold atoms inside an optical cavity in system (1)^{37,38}, the finite size effects may also become important and experimentally observable in near future experiments on system (1). As advocated in²¹, the Hamiltonian Eqn.1 with independent g and g' is the generic Hamiltonian describing various experimental systems under the two atomic levels and a single photon mode approximation. In²¹, by the $1/J$ expansion, we focused on the $U(1)/Z_2$ Dicke model Eqn.1 near the $U(1)$ limit (namely, with a small anisotropy parameter $g'/g = \beta \ll 1$ and not too far from the critical strength g_c) at any finite N . In a very recent preprint³⁹, by the strong coupling expansion and the ED, the authors studied the $U(1)/Z_2$ Dicke model in its dual presentation starting from the Z_2 limit $\beta = 1$. Here, by the $1/J$ expansion and ED, we will study the $U(1)/Z_2$ Dicke model Eqn.1 starting from the $U(1)$ limit $\beta = 0$ which is complementary to the strong coupling expansion in³⁹. The combinations of both approaches will lead to rather complete understandings of the $U(1)/Z_2$ Dicke model Eqn.1 in the full range of $0 < \beta < 1$.

In this paper, we study novel quantum phenomena in the $U(1)/Z_2$ Dicke model Eqn.1 in its spin $J = N/2$ representation at a finite N , any interaction strength g and anisotropy parameter $0 < \beta < 1$ by the $1/J$ expansion²¹ and the ED^{13,21}. As a fixed β , as the g increases, we identify 3 crossover regimes: the normal, $U(1)$ and the quantum tunneling (QT) regime Fig.2. The super-radiant regime at $N = \infty$ splits into the two regimes at a finite N : the $U(1)$ and quantum tunneling (QT) regime. In the $U(1)$ regime, we perform a (non-)degenerate perturbation to evaluate the energy spectrum. It is the Berry phase which leads to the level crossings between the even and odd parity, therefore the alternating parities on the ground state and excited states. In the QT regime, by the WKB method, we find the emergencies of bound states one by one as the interaction strength increases, then investigate a new class of quantum tunneling processes through the instantons between the two bound states in the compact photon phase. It is the Berry phase interference effects in the instanton tunneling event which leads to Schrodinger Cats oscillating with even and odd parities in both ground and higher energy bound states. We map out the energy level evolution from the $U(1)$ to the QT regime. In the $U(1)$ regime, the doublets consist of scattering states organized as $(e, o), (o, e), \dots$ (or $(o, e), (e, o), \dots$) pattern. While in the QT regime, the doublets consist of bound states (or Schrodinger Cats) organized as $(e, o), (e, o), \dots$ (or $(o, e), (o, e), \dots$) pattern.

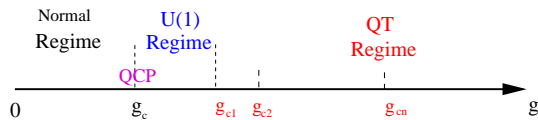


FIG. 2. The three regimes of the $U(1)/Z_2$ Dicke model at a finite N as the coupling g increases at a fixed anisotropy parameter $0 < g'/g = \beta < 1$. The normal regime, the $U(1)$ regime and the quantum tunneling (QT) regime. The quantum critical point (QCP) at $N = \infty$ is at $g_c = \sqrt{\omega_a \omega_b} / (1 + \beta)$. The superradiant regime at $N = \infty$ splits into the $U(1)$ regime and the QT regime at a finite N . The dynamic variables in the three regimes are: a, b in the normal regime, $\delta\rho_a, e^{i\theta_a}$ in the $U(1)$ regime and $\delta\rho_a, \theta_a, \tau_z$ in the QT regime. As shown in the text, there exists some duality relations between the $U(1)$ regime and the QT regime. The strong coupling expansion in³⁹ works very well in the QT regime and also $U(1)$ regime not too close to the QCP. The $U(1)$ regime may disappear if β gets too close to 1.

There are also some sort of duality relations between the two regimes in both Hamiltonian and spectrum. We compute the photon correlation functions, squeezing spectrum and number correlation functions in both regimes which can be detected by Fluorescence spectrum, phase sensitive homodyne detection and Hanbury-Brown-Twiss (HBT) type of experiments respectively⁴⁰. When comparing the results with those achieved from the strong coupling expansion in³⁹, we find nearly perfect agreements among the $1/J$ expansion, the strong coupling expansion and the ED not only in the QT regime, but also in the $U(1)$ regime not too close to the QCP at $N = \infty$. The combination of the three methods lead to rather complete physical pictures in the whole crossover regimes from the $U(1)$ Dicke to the Z_2 Dicke model in Fig.2. Experimental realizations, especially the preparations and detections of the Schrodinger Cats in both experimental systems are discussed. Connections with the previous works are speculated and future perspectives are outlined.

II. $1/J$ EXPANSION IN THE SUPER-RADIANT PHASE.

The $U(1)/Z_2$ Dicke model^{21,22} is described by:

$$H_{U(1)/Z_2} = \omega_a a^\dagger a + \omega_b J_z + \frac{g}{\sqrt{2J}} (a^\dagger J_- + a J_+) + \frac{g'}{\sqrt{2J}} (a^\dagger J_+ + a J_-) \quad (1)$$

where the ω_a, ω_b are the cavity photon frequency and the energy difference of the two atomic levels respectively, the $g = \sqrt{N}\tilde{g}$, $N = 2J$ is the collective photon-atom rotating wave (RW) coupling. The $g' = \sqrt{N}\tilde{g}'$ is the counter-rotating wave (CRW) term. We fix their ratio to be $0 < g'/g = \beta < 1$. If $\beta = 0$, Eqn.1 reduces to the $U(1)$ Dicke model^{20,21} with the $U(1)$ symmetry $a \rightarrow$

$ae^{i\theta}, \sigma^- \rightarrow \sigma^- e^{i\theta}$ leading to the conserved quantity $P = a^\dagger a + J_z$. The CRW g' term breaks the $U(1)$ to the Z_2 symmetry $a \rightarrow -a, \sigma^- \rightarrow -\sigma^-$ with the conserved parity operator $\Pi = e^{i\pi(a^\dagger a + J_z)}$. If $\beta = 1$, it becomes the Z_2 Dicke model^{13,14}.

Following²¹, inside the super-radiant phase, it is convenient to write both the photon and atom in the polar coordinates $a = \sqrt{\lambda_a^2 + \delta\rho_a} e^{i\theta_a}, b = \sqrt{\lambda_b^2 + \delta\rho_b} e^{i\theta_b}$. When performing the controlled $1/J$ expansion, we keep the terms to the order of $\sim j, \sim 1$ and $\sim 1/j$, but drop orders of $1/j^2$ or higher. We first minimize the ground state energy at the order j and found the saddle point values of λ_a and λ_b :

$$\lambda_a = \frac{g + g'}{\omega_a} \sqrt{\frac{j}{2}(1 - \mu^2)}, \quad \lambda_b = \sqrt{j(1 - \mu)} \quad (2)$$

where $\mu = \omega_a \omega_b / (g + g')$. In the superradiant phase $g + g' > g_c = \sqrt{\omega_a \omega_b}$. In the normal phase $g + g' < g_c$, one gets back to the trivial solution $\lambda_a = \lambda_b = 0$.

Observe that (1) in the superradiant phase $g(1 + \beta) > g_c$, $\lambda_a^2 \sim \lambda_b^2 \sim j$, (2) it is convenient to introduce the \pm modes: $\theta_\pm = (\theta_a \pm \theta_b)/2, \delta\rho_\pm = \delta\rho_a \pm \delta\rho_b, \lambda_\pm^2 = \lambda_a^2 \pm \lambda_b^2$. (3) Defining the Berry phase in the + sector²⁰ as $\lambda_+^2 = P + \alpha$ where $P = 1, 2, \dots$ is the closest integer to the λ_+^2 , so $-1/2 < \alpha < 1/2$. Due to the large gap in the θ_- , it is justified to drop the Berry phase in the - sector. (4) after shifting $\theta_\pm \rightarrow \theta_\pm + \pi/2$, we reach the Hamiltonian to the order of $1/j$:

$$\mathcal{H}[\delta\rho_\pm, \theta_\pm] = \frac{D}{2} (\delta\rho_+ - \alpha)^2 + D_- [\delta\rho_- + \gamma(\delta\rho_+ - \alpha)]^2 + 4\omega_a \lambda_a^2 \left[\frac{1}{1 + \beta} \sin^2 \theta_- + \frac{\beta}{1 + \beta} \sin^2 \theta_+ \right] \quad (3)$$

where $D = \frac{2\omega_a(g+g')^2}{E_H^2 N}$ is the phase diffusion constant in the + sector, $D_- = E_H^2 / 16 \lambda_a^2 \omega_a$ with $E_H^2 = (\omega_a + \omega_b)^2 + 4(g+g')^2 \lambda_a^2 / N$. The $\gamma = \frac{\omega_a^2}{E_H^2} (1 - \frac{(g+g')^4}{\omega_a^4})$ is the coupling between the + and - sector.

Note that the large J expansion condition is $\lambda_a^2 \gg 1$. In the $j \rightarrow \infty$ limit, it holds for any $g > g_c$, but leads to a constraint on g at a finite j . In the superradiant regime, one can simply set $\sin^2 \theta_\pm \sim \theta_\pm^2$ in Eqn.3 which becomes a quadratic theory. It can be easily diagonalized and lead to one low energy gapped pseudo-Goldstone mode and a high energy gapped optical mode. Setting $\beta = 1$ recovers the results for the Z_2 Dicke model in the superradiant phase at $N = \infty$ in¹³.

If one neglects the quantum fluctuations of the θ_- mode, namely, by setting θ_- at its classical value $\theta_- = 0$, Eqn.3 is simplified to:

$$\mathcal{H}_+[\delta\rho_+, \theta_+] = \frac{D}{2} (\delta\rho_+ - \alpha)^2 + 2\omega_a \lambda_a^2 \frac{2\beta}{1 + \beta} \sin^2 \theta_+ \quad (4)$$

where $[\theta_+, \delta\rho_+] = i\hbar$. In the superradiant limit $4\lambda_a^2 \frac{\beta}{1 + \beta} \gg 1$, one can identify the approximate atomic

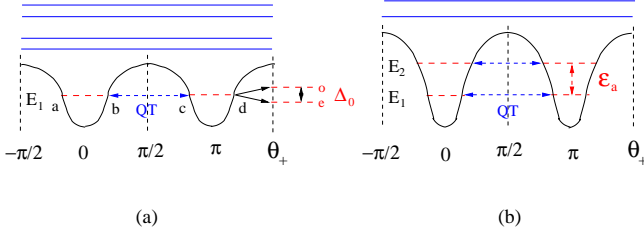


FIG. 3. The bound states and the quantum tunneling processes in the QT regime in Fig.2. The atomic energy ϵ_a and the tunneling energy Δ_0 are shown. But the higher optical energy ϵ_o is not shown. (a) At $g = g_{c1} > g_c = \sqrt{\omega_a \omega_b} / (1 + \beta)$, the double well potential in the θ_+ sector in Eqn.4 holds just one bound state with energy E_1 denoted by a red dashed line. The blue dashed line shows the quantum tunneling between the two bound states which leads to the splitting Δ_0 listed in Eqn.16. The blue solid lines denote scattering states shown in Fig.5a,4b (b) As the g increases further to $g = g_{c2} > g_{c1}$, the lowest two scattering states in (a) also become the second bound state with energy $E_2 = E_1 + \epsilon_a$, the third bound state shows up at $g = g_{c3} > g_{c2} > g_{c1}$ and so on (see also Fig.4). The excitation energy is the "atomic" energy ϵ_a . As explained below Eqn.15, the ground state could also be odd parity depending on $(-1)^P$.

mode:

$$\omega_{-0}^2 = 4\omega_a \lambda_a^2 \frac{2\beta}{1+\beta} D = \frac{4}{E_H^2} \frac{\beta}{1+\beta} [(g+g')^4 - g_c^4] \quad (5)$$

which is nothing but the pseudo-Goldstone mode due to the CRW g' term.

Note that for small $\beta < 1$, the condition to reach the superradiant regime $4\lambda_a^2 \frac{\beta}{1+\beta} \gg 1$ is more stringent than the large J expansion condition $\lambda_a^2 \gg 1$.

By neglecting the quantum fluctuations of θ_- , the high energy optical mode in the θ_- sector can not be seen anymore in Eqn.4. The approximation may not give very precise numbers to physical quantities, but do lead to correct qualitative physical picture, especially the topological effects due to the Berry phase in all the physical quantities.

III. $U(1)$ REGIME AND THE FORMATION OF CONSECUTIVE BOUND STATES IN QUANTUM TUNNELING REGIME.

As the potential in the θ_+ sector in Eqn.4 gets deeper and deeper, there are consecutive bound states formations at $g_c < g_{c1} < g_{c2} \dots$ leading to the "atomic" energy scale ϵ_a . The QT regime in Fig.2 is signatred by the first appearance of the bound state after which there are consecutive appearances of more bound states at higher energies (Fig.3a,b). The regime $g_c < g < g_{c1}$ is the $U(1)$ regime in Fig.2.

One can calculate all these $g_c < g_{c1} < g_{c2} \dots$ by using the Bohr-Sommerfeld quantization condition for a smooth potential $\int_a^b p d\theta = (n + 1/2)\pi\hbar$, $n = 0, 1, 2, \dots$

where $p = \sqrt{2m(E_{n+1} - V(\theta))}$ and the $E_{n+1} = E_1, E_2, \dots$ is the $(n + 1) - th$ bound state energy in Fig.3a,b. From Eqn.4, we can see the $m = \frac{1}{D}$, $V(\theta) = \omega_a \lambda_a^2 \frac{2\beta}{1+\beta} (1 - \cos 2\theta_+)$ and the a and b are the two end points shown in Fig.3a. We find that the bound states emerge at

$$\frac{\omega_{-0}}{D} = (n + 1/2) \frac{\pi}{2} \hbar, \quad n = 0, 1, 2, \dots \quad (6)$$

In Eqn.6, setting $n = 0$, one can see when $\frac{\omega_{-0}}{D} < \frac{\pi}{4} \hbar$, there is no bound state. This is the $U(1)$ regime in Fig.2. Substituting the expression for the phase diffusion constant D and the atomic mode ω_{-0} in Eqn.5 leads to the condition for the $U(1)$ regime:

$$4\lambda_a^2 \sqrt{\frac{\beta}{1+\beta}} < \frac{\pi}{4} \quad (7)$$

Note that for large J expansion to apply, one only need to require $\lambda_a^2 > 1$, So for sufficiently small $g'/g = \beta$, there is an appreciable $U(1)$ regime $g_c < g < g_{c1}$ before the quantum tunneling (QT) regime in Fig.2.

In this $U(1)$ regime, the second term in Eqn.4 breaks the $U(1)$ symmetry to Z_2 symmetry, the Goldstone mode at $N = \infty$ simply becomes a pseudo-Goldstone mode²⁰⁻²². But its effects at a finite N is much more delicate to analyze. One can treat the second term in Eqn.4 perturbatively either by a non-degenerate at $\alpha \neq 0$ or degenerate perturbation expansion at $\alpha = 0$. The total excitation P is not conserved anymore and is replaced by the conserved parity $\Pi = (-1)^P$, the energy levels are only grouped into even and odd parities in Fig.4. As shown in²¹, at a given sector P , $m = 0, \pm 1, \dots, \pm P$ at $\alpha = 0$, a first order degenerate perturbation at $m = \pm 1$ leads to the maximum splitting at $\alpha = 0$ in Fig.4b:

$$\Delta_{m=\pm 1, U(1)}(\alpha = 0) = \frac{D}{2} - \frac{\omega_a \lambda_a^2}{2} \frac{2\beta}{1+\beta} \quad (8)$$

Using Eqn.5, one can rewrite $\Delta = \frac{D}{2} [1 - \frac{1}{2} (\frac{\omega_{-0}}{D})^2] > 0$. For general $\pm m$, one needs $m - th$ order (with the constraint $|m| \leq P$ in a given sector P) degenerate perturbation calculation to find the the maximum splitting $\Delta_{m, U(1)}$ at $\alpha = 0$ between the m and $m + 1$ crossing in Fig.4b:

$$\Delta_{m, U(1)}(\alpha = 0) = D(m + \frac{1}{2}) - R_{m+1} - R_m \quad (9)$$

where $R_m \sim (\frac{\omega_a \lambda_a^2}{2} \frac{2\beta}{1+\beta})^m$, $m = 0, 1, \dots, P$; $R_0 = 0$ is the gap opening at the $m+1$ crossing in the $U(1)$ limit Fig.4a. Setting $m = 0$ recovers Eqn.8.

Note that the degenerate pair $(m, -m-1)$ at the edge at $\alpha = \pm 1/2$ has different parity, so will not be mixed in any order of perturbations²¹. It is easy to compute the edge gap at $\alpha = \pm 1/2$ by a non-degenerate perturbation. Obviously, the second term in Eqn.4 connects only $\Delta m = \pm 2$, so the first order perturbation vanishes,

one need to get to at least second order non-degenerate perturbation²¹. There could also be a slight shift in the crossing point between the two opposite parities at $(m, -m - 1)$

$$\Delta_{m,U(1)}(\alpha = \pm 1/2) = D(m + 1) - S(m) \quad (10)$$

where $S(m) \sim (\frac{\omega_a \lambda_a^2}{2} \frac{2\beta}{1+\beta})^2$. It leads to $D, 2D, 3D, \dots$ at $m = 0, 1, 2, \dots$ at the $U(1)$ limit $\beta = 0$ shown in Fig.4a. It is easy to see that at a given m -th doublet the maximum gap at $\alpha = 0$ is smaller than the edge gap at $\alpha = \pm 1/2$, $\Delta_{m,U(1)}(\alpha = 0) < \Delta_{m,U(1)}(\alpha = \pm 1/2)$. But both are of the same order.

Nonetheless, the important phenomena of Goldstone and Higgs mode at the $U(1)$ limit can still be observed in this $U(1)$ regime after considering these degenerate and non-degenerate perturbations. Various photon correlation functions in this $U(1)$ regime can be evaluated straightforwardly²¹.

Now we follow the formation of the bound states just after the $U(1)$ regime. When $\frac{\omega_{-0}}{D} = \frac{\pi}{4}\hbar$, namely $g = g_{c1}$, it just holds the first bound state with $\theta_b = -\theta_a = \frac{\pi}{2}$, $E_1 = 2\omega_a \lambda_a^2 \frac{2\beta}{1+\beta}$. When $\frac{\pi}{4}\hbar < \frac{\omega_{-0}}{D} < \frac{3\pi}{4}\hbar$, it holds the first bound state (Fig.3a) with energy $E_1 = 2\omega_a \lambda_a^2 \frac{2\beta}{1+\beta} \sin^2 \theta_a$ where $\frac{\omega_{-0}}{D} F(\theta_a) = \frac{\pi}{4}\hbar$, $F(\theta_a) = \int_0^{\theta_a} d\theta \sqrt{\sin^2 \theta_a - \sin^2 \theta}$, $0 < \theta_a < \pi/2$. It is easy to see $0 < F(\theta_a) < 1$, $F(\theta_a = \pi/2) = 1$.

IV. QUANTUM TUNNELING BETWEEN THE TWO BOUND STATES: BERRY PHASE AND INSTANTONS.

The instanton solution for a Sine-Gordon model was well known⁴². From Eqn.4, we can find the classical instanton solution connecting the two minima from $\theta_+ = 0$ or $\theta_+ = \pi$: $\theta_+(\tau) = 2 \tan^{-1} e^{\omega_{-0}(\tau - \tau_0)}$ where τ_0 is the center of the instanton. Its asymptotic form as $\tau \rightarrow \infty$ is $\theta_+(\tau \rightarrow \infty) \rightarrow \pi - 2e^{-\omega_{-0}(\tau - \tau_0)}$. The corresponding classical instanton action is:

$$S_0 = \frac{2\omega_{-0}}{D} \quad (13)$$

The instanton problems in the three well known systems (1) a double well potential (DWP) in a ϕ^4 theory (2) periodic potential problem (PPP) (3) a particle on a circle (POC) are well documented in⁴². The tunneling problem in the present problem is related, but differ-

When $\frac{\omega_{-0}}{D} = \frac{3\pi}{4}\hbar$, namely $g = g_{c2}$, it just holds the second bound state with $\theta_b = -\theta_a = \frac{\pi}{2}$, $E_2 = 2\omega_a \lambda_a^2 \frac{2\beta}{1+\beta}$. While the first bound state energy is given by $F(\theta_a) = 1/3$, $E_1 = 2\omega_a \lambda_a^2 \frac{2\beta}{1+\beta} \sin^2 \theta_a$. When $\frac{3\pi}{4}\hbar < \frac{\omega_{-0}}{D} < \frac{5\pi}{4}\hbar$, it holds two bound states (Fig.3b) with the energies:

$$\begin{aligned} E_1 &= 2\omega_a \lambda_a^2 \frac{2\beta}{1+\beta} \sin^2 \theta_{1a}, & \frac{\omega_{-0}}{D} F(\theta_{1a}) &= \frac{\pi}{4}\hbar \\ E_2 &= 2\omega_a \lambda_a^2 \frac{2\beta}{1+\beta} \sin^2 \theta_{2a}, & \frac{\omega_{-0}}{D} F(\theta_{2a}) &= \frac{3\pi}{4}\hbar \end{aligned} \quad (11)$$

where one can identify the first atomic energy in Fig.3b:

$$\epsilon_a = E_2 - E_1 = 2\omega_a \lambda_a^2 \frac{2\beta}{1+\beta} (\sin^2 \theta_{2a} - \sin^2 \theta_{1a}) \quad (12)$$

As expected ϵ_a is different than the ω_{-0} in Eqn.5.

As $g \rightarrow \infty$, $D \rightarrow 0$, while $\omega_{-0} \rightarrow \sqrt{2}\omega_a \sqrt{\frac{2\beta}{1+\beta}}$, so the left hand side of Eqn.6 diverges, there are infinite number of bound states shown in Fig.4e.

Note that because the bound state is either localized around $\theta_+ = 0$ or $\theta_+ = \pi$, so the Berry phase α in Eqn.4 plays no roles, so can be dropped. However, as to be shown in the following section, it does play very important roles in the quantum tunneling process between the two bound states shown in Fig.3 and 5.

ent than all the three systems in the following important ways: (1) the potential $V(\theta) = 2\omega_a \lambda_a^2 \frac{2\beta}{1+\beta} (1 - \cos 2\theta_+)$ in Eqn.4 is a periodic potential in θ_+ . In this regard, it is different than the ϕ^4 theory, but similar to PPP. (2) The θ_+ is a compact angle confined in $0 < \theta_+ < 2\pi$. In this regard, it is different than the PPP, but similar to POC. (3) There are two minima inside the range $0 < \theta_+ < 2\pi$ instead of just one. In this regard, it is different than the POC, but similar to the ϕ^4 theory. So the present quantum tunneling problem is a new class one. Furthermore, it is also very important to consider the effects of Berry phase which change the action of instanton to $S_{int} = S_0 + i\alpha\pi$, that of anti-instanton to $\bar{S}_{int} = S_0 - i\alpha\pi$ (Fig.5) where $-1/2 < \alpha < 1/2$ is the Berry phase in Eqn.4.

Taking into account the main differences of the present QT problem from the DWP, PPP and POC studied perviously⁴², especially the crucial effects of the Berry phase, we can evaluate the transition amplitude from $\theta_+ = 0$ to $\theta_+ = \pi$ in Fig.5:

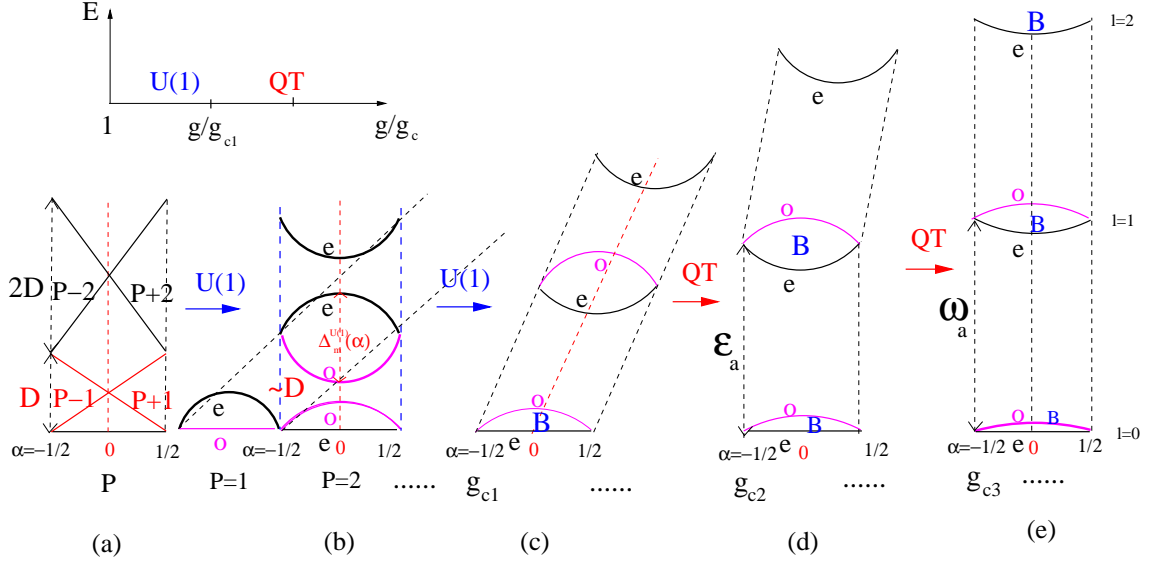


FIG. 4. The atomic energy level evolution from the $U(1)$ regime to the QT regime as g changes at a fixed β . The ground state energy has been subtracted. D is the phase diffusion constant. In the $U(1)$ regime in (a) and (b), there are P doublets along the vertical (blue dashed) lines. (a) The energy spectrum at the $U(1)$ limit $\beta = 0^{21}$. (b) The energy level repulsions between the same parity at $\alpha = 0$ and level crossings at $\alpha = \pm 1/2$ between the opposite parities in the $U(1)$ regime. The maximum splitting at $\alpha = 0$ and the gap at the edge $\alpha = \pm 1/2$ are given by Eqn.9 and 10 respectively. All the states are scattering states. If the total excitation P is even, along the vertical (blue dashed) lines, the doublets are organized as $(e, o), (o, e), (e, o), (o, e), \dots$ (see also Fig.6a). If P is odd, one need flip all the parities. See Fig.7a,8a at $N = 2, \beta = 0.1$. If we follow the states with $P, P+1, P+2, \dots$ at $l = 0, 1, 2, \dots$ respectively, then the doublets are organized as $(e, o), (e, o), \dots$, there are relatively large shifts of zeros to the right delineated by the black dashed line. Only the splittings at $m = \pm 1, \pm 2$ at $P = 1, 2$ are shown here. See Fig.7b,8b at $N = 2, \beta = 0.5$. (c) The doublet at $l = 0$ becomes the first bound state (Schrodinger cat) denoted as B at $g = g_{c1}$, while the states at $l = 1, \dots$ remain scattering states as shown in Fig.3a,5a. (d) The doublet at $l = 1$ becomes the second bound state at $g = g_{c2}$, the two bound states at $l = 0, 1$ are connected by nearly straight boundaries at $\alpha = -1/2, 0, 1/2$. The states at $l = 2, \dots$ remain scattering states as shown in Fig.3b. See Fig.7c,8c at $N = 2, \beta = 0.9$. (e) Finally, more states become bound states at $g = g_{c3}, \dots$ where the energy level pattern becomes $(e, o), (e, o), \dots$ in the QT regime (see also Fig.6b). If P is odd, one need also flip all the parities. There is a shift by exact one period from (b) to (e). Intuitively, a leaning tower with infinite stories gradually becomes straight as the system evolves from the $U(1)$ regime to the QT regime. The maximum splitting at $\alpha = 0$ are given by Eqn.8,9 for scattering states, Eqn.16,17, for bound states (Schrodinger cats) and decrease from (b) to (e). The edge gap at $\alpha = \pm 1/2$ are given by Eqn.10 and the atomic energy ϵ_a in Fig.3b for scattering states and bound states respectively and increases from (b) to (e), but starts to become flat since the second bound state forms at $l = 1$ in (d). The maximum gap at $\alpha = 0$ is comparable to the edge gap at $\alpha = \pm 1/2$ in the $U(1)$ regime (b), but much smaller in the QT regime where $\Delta_l \ll \omega_a$ (d). This evolution from (b) to (e) is precisely observed in the ED in Fig.7 and fine structures in all the doublets at $l = 0, 1, 2$ in Fig.8. The higher energy optical modes are not shown. As said in the caption of Fig.2, the $U(1)$ regime disappears if β gets too close to 1 as shown in Fig.7c,8c.

$$\begin{aligned}
\langle \pi | e^{-H\tau} | 0 \rangle &= \left(\frac{\omega_{-0}}{\pi D \hbar} \right)^{1/2} e^{\omega_{-0}\tau/2} \sum_{n_1, n_2} \frac{(JK e^{-S_{int}\tau})^{n_1}}{n_1!} \frac{(JK e^{-\bar{S}_{int}\tau})^{n_2}}{n_2!} \delta_{n_1 - n_2, odd} \\
&= \left(\frac{\omega_{-0}}{\pi D \hbar} \right)^{1/2} e^{\omega_{-0}\tau/2} \frac{1}{2} [e^{2JK\tau e^{-S_0} \cos \alpha \pi} - e^{-2JK\tau e^{-S_0} \cos \alpha \pi}]
\end{aligned} \tag{14}$$

where n_1 (n_2) is sum over the instanton (anti-instanton), $J = (S_0/2\pi\hbar)^{1/2}$ is given by the instanton action in Eqn.13 and K is the ratio of two relevant determinants to remove the zero mode of the instantons due to its center τ_0 listed above Eqn.13. It can be shown that $K = C_0\omega_{-0}$ where $C_0 = 2$ is extracted from the asymptotic form of the instanton solution in the $\tau \rightarrow \infty$ limit listed above Eqn.13. Similarly, in finding the transition amplitude

from 0 back to 0, one only need to change $\delta_{n_1 - n_2, odd}$ to $\delta_{n_1 - n_2, even}$ in the first line, consequently, the $-$ sign to the $+$ sign in the second line in Eqn.14.

The two transition amplitudes lead to the Schrodinger

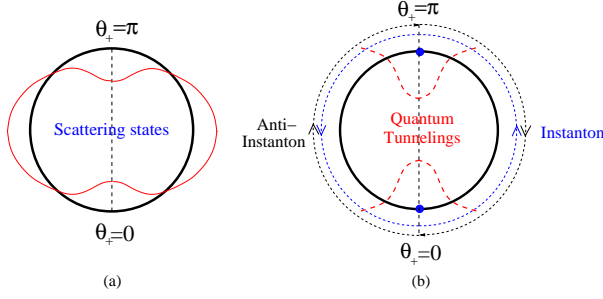


FIG. 5. (a) Scattering states: There is a global phase wandering around the θ_+ circle from 0 to 2π with the phase diffusion constant D . See Fig.4b, Fig.8a,b. (b) Bound states (Schrodinger cats): The quantum tunneling process due to the instantons between the two bound states at $\theta_+ = 0$ and $\theta_+ = \pi$. The counterclockwise (blue dashed line) tunneling is an instanton. The clockwise (black dashed line) tunneling is an anti-instanton. It is the Berry phase which leads to the oscillations of parities in the ground state and excited states. See Fig.4c,d,e, Fig.8c.

” Cat ” state with even/odd parity:

$$\begin{aligned} |e\rangle_{0,SC} &= \frac{A}{\sqrt{2}}(|\theta_+ = 0\rangle + |\theta_+ = \pi\rangle), \\ |o\rangle_{0,SC} &= \frac{A}{\sqrt{2}}(|\theta_+ = 0\rangle - |\theta_+ = \pi\rangle), \end{aligned} \quad (15)$$

where the overlapping coefficient is $A^2 = |\langle x = 0 | n = 0 \rangle|^2 = (\frac{\omega_{-0}}{\pi\hbar D})^{1/2}$. They have the energy $E_{e/o} = \frac{\hbar\omega_{-0}}{2} \mp \Delta_0/2$ with the splitting between them given by:

$$\begin{aligned} \Delta_0(\alpha) &= 8\omega_{-0}(\cos \alpha\pi)(\frac{\omega_{-0}}{\pi D})^{1/2} e^{-\frac{2\omega_{-0}}{D}} \\ &\sim (\cos \alpha\pi)\sqrt{N}e^{-cN} \end{aligned} \quad (16)$$

where one can see that it is the Berry phase which leads to the oscillation of the gap and parity in Eqn.15. It vanishes at the two end points $\alpha = \pm 1/2$ and reaches maximum at the middle $\alpha = 0$. Note that the Berry phase α is defined^{20,21} at a given sector P . So Eqn.15 has a background parity $\Pi = (-1)^P$. So there is an infinite number of oscillating parities in Eqn.15 as g increases.

Because the Berry phase effects remain in the given P sector, extending the results in Ref.⁴³, we find the splitting in the n -th excited bound states ($n = 0, 1$ in Fig.3b):

$$\Delta_n(\alpha) = \frac{1}{n!} \left(\frac{8\omega_{-0}}{D}\right)^n \Delta_0 \quad (17)$$

where $n = 0, 1, 2, \dots$ with the corresponding n -th Schrodinger ”Cat ” state with even/odd parity and the energy $E_{e/o,n} = (n + \frac{1}{2})\hbar\omega_{-0} \mp \Delta_n/2$:

$$\begin{aligned} |e\rangle_{n,SC} &= \frac{1}{\sqrt{2}}(|n\rangle_L + |n\rangle_R), \\ |o\rangle_{n,SC} &= \frac{1}{\sqrt{2}}(|n\rangle_L - |n\rangle_R), \end{aligned} \quad (18)$$

where $|n\rangle_{L/R}$ is the n -th bound state in the left(right) well in Fig.3a,b. Putting $n = 0$ and projecting it to the coordinate space at $x = 0$ recovers Eqn.15 (Note that the projection to $x = 0$ does not work for n is odd). One can see the higher the bound state in the Fig.3, the larger the splitting is. The main difference than the energy level pattern in the $U(1)$ regime is that all the bound states have the $(e, o), (e, o), \dots$ (or $(o, e), (o, e), \dots$) pattern shown in Fig.4d,e and Fig.6b. This important observation is completely consistent with the results achieved from the strong coupling expansion in³⁹ after identifying $n \sim l$. For example, as explained in³⁹, there is an extra oscillating sign $(-1)^l$ in Eqn.5 in³⁹ achieved from the strong coupling expansion, which is crucial to reconcile the results achieved from the two independent approaches !

V. PHOTON, SQUEEZING AND NUMBER CORRELATION FUNCTIONS

Following the procedures for the $U(1)$ Dicke model at $\beta = 0$ in²¹, treating the second term in Eqn.4 as a small perturbation when β is small, using non-degenerate perturbation away from $\alpha = 0$ and degenerate perturbation near $\alpha = 0$ one can evaluate Photon, squeezing and number correlation functions in the $U(1)$ regime outlined in Fig.6a. Here we focus on calculating these correlation functions in the QT regime outlined in Fig.6b.

The above physical pictures in the QT regime inspire us to decompose photon and atomic operators as:

$$a = a_L\tau_z, \quad b = -b_L\tau_z \quad (19)$$

where $a_L = \sqrt{\lambda_a^2 + \delta\rho_a}e^{i\theta_a}$, $b_L = \sqrt{\lambda_b^2 + \delta\rho_b}e^{i\theta_b}$ are confined to the left well in Fig.3 and the $\tau_z = \pm 1$ stand for the Left/Right quantum wells in Fig.3. It is the τ_z component which contains the important Berry phase effects and the quantum tunneling process between the Left and Right quantum well with the tunneling Hamiltonian $H_T = \Delta_l\tau_x$. Note that the two states $\tau_z = \pm 1$ here is the two Schrodinger Cat states of the strongly interacting atom-photon system instead of the two levels of an atom $\sigma_z = \pm 1$ in the original $U(1)/Z_2$ Dicke Hamiltonian Eqn.1. The two energies Δ_l and ϵ_a should appear in the single photon correlation function (which contain the magnitude $\delta\rho_a$, the phase θ_a and the Ising τ_z correlation functions as shown in Fig.2) with the corresponding spectral weights $\sim N, \sim 1$ respectively. By using this decomposition, we will perform the $1/J$ expansion to evaluate all the relevant photon and atomic correlation functions.

Because the Z_2 symmetry is broken in either left or right well in Fig.3, one can ignore the periodicity in θ_a, θ_b

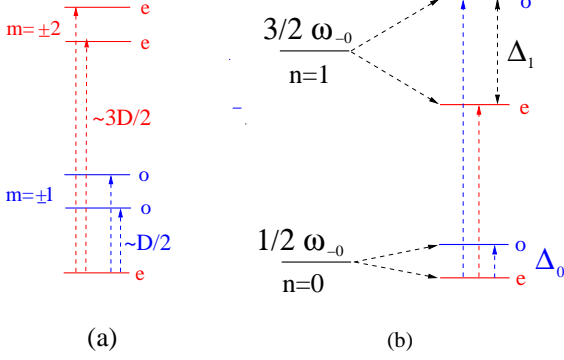


FIG. 6. Splittings near the Berry phase $\alpha = 0$ in the (a) $U(1)$ regime in Fig.4b and Fig.5a. D is the diffusion constant^{20,21}. $m = \pm 1, \pm 2, \dots$ are the magnetic quantum numbers. (b) the QT regime in Fig.4d and Fig.5b. The ground state $n = 0$ and the first excited state $n = 1$ and their splittings Δ_0 and Δ_1 due to the quantum tunnelings of instantons subject to the Berry phase. The blue and red transition lines can be mapped out by photon and photon number correlation functions respectively. Shown is the background parity $(-1)^P$ is even (e). When $(-1)^P$ is odd (o), one just changes even and odd in the figure.

and expand the atom and photon operators as:

$$\begin{aligned}
 a_L &= \lambda_a + i\lambda_a\theta_a + \frac{\delta\rho_a}{2\lambda_a} - \frac{\lambda_a\theta_a^2}{2} - \frac{(\delta\rho_a)^2}{8\lambda_a^3} + \dots \\
 b_L &= \lambda_b + i\lambda_b\theta_b + \frac{\delta\rho_b}{2\lambda_b} - \frac{\lambda_b\theta_b^2}{2} - \frac{(\delta\rho_b)^2}{8\lambda_b^3} + \dots \quad (20)
 \end{aligned}$$

Using the Holstein-Primakoff (HP) representation of the angular momentum operator $J_z = b^\dagger b - J$, $J_+ = b^\dagger\sqrt{2J - b^\dagger b}$, $J_- = \sqrt{2J - b^\dagger b}b$, one can evaluate the atomic spin correlation functions. Here, we focus on evaluating the photon correlation functions.

Using Eqn.4, 5, we can calculate the phase-phase, density-density and density-phase correlation functions in the imaginary time τ :

$$\begin{aligned}
 \langle \theta_a(\tau)\theta_a(0) \rangle &= \frac{D}{2\omega_{-0}} e^{-\omega_{-0}\tau}, \quad \langle \theta_a^2 \rangle = \frac{D}{2\omega_{-0}} \\
 \langle \delta\rho_a(\tau)\delta\rho_a(0) \rangle &= \frac{\omega_a\lambda_a^2}{2\omega_{-0}} \frac{2\beta}{1+\beta} e^{-\omega_{-0}\tau}, \quad \langle (\delta\rho_a)^2 \rangle = \frac{\omega_a\lambda_a^2}{2\omega_{-0}} \frac{2\beta}{1+\beta} \\
 \langle \delta\rho_a(\tau)\theta_a(0) \rangle &= -\frac{i}{4} e^{-\omega_{-0}\tau} = -\langle \delta\theta_a(\tau)\rho_a(0) \rangle \quad (21)
 \end{aligned}$$

Because the θ_+ is a phase confined on $0 < \theta_+ < 2\pi$, we can define $q = e^{i\theta_+}$. For $\theta_+ = 0, \pi$, we can set $q = \tau_z$ standing for the left/right well in Fig.3 and find the correlation function in the l -th state:

$$\langle e|\tau_z(\tau)\tau_z(0)|e \rangle = e^{-\Delta_l\tau} \quad (22)$$

where Δ_l is the splitting at l -th state in Fig.3 and 6.

From the decomposition Eqn.19, 20, 21 and Eqn.22, one can evaluate the photon correlation functions:

$$\begin{aligned}
 \langle a(\tau)a^\dagger(0) \rangle &= [\lambda_a^2 - \frac{\omega_{-0}}{8\omega_a} (\frac{1+\beta}{2\beta}) - \frac{\omega_a}{8\omega_{-0}} (\frac{2\beta}{1+\beta})] e^{-\Delta_0\tau} \\
 &+ \frac{1}{8} [\frac{\omega_{-0}}{\omega_a} (\frac{1+\beta}{2\beta}) + \frac{\omega_a}{\omega_{-0}} (\frac{2\beta}{1+\beta}) - 2] e^{-(\omega_{-0}+(\Delta_1+\Delta_0)/2)\tau} \quad (23)
 \end{aligned}$$

where the first term containing the ground state splitting Δ_0 has the corresponding spectral weight $\sim N$, while the second term containing the atomic energy ϵ_a plus the average of the splittings at $n = 0$ and $n = 1$ in Fig.6 has the spectral weight ~ 1 .

Very similarly, one can evaluate the anomalous photon correlation functions:

$$\begin{aligned}
 \langle a(\tau)a(0) \rangle &= [\lambda_a^2 - \frac{\omega_{-0}}{8\omega_a} (\frac{1+\beta}{2\beta}) - \frac{\omega_a}{8\omega_{-0}} (\frac{2\beta}{1+\beta})] e^{-\Delta_0\tau} \\
 &+ \frac{1}{8} [\frac{\omega_a}{\omega_{-0}} (\frac{2\beta}{1+\beta}) - \frac{\omega_{-0}}{\omega_a} (\frac{1+\beta}{2\beta})] e^{-(\omega_{-0}+(\Delta_1+\Delta_0)/2)\tau} \quad (24)
 \end{aligned}$$

where the first term containing the ground state splitting Δ_0 has the same spectral weight $\sim N$ as its counterpart in Eqn.23, while the second term containing the atomic energy ϵ_a plus the average of the splittings at $n = 0$ and $n = 1$ in Fig.6 has a different spectral weight ~ 1 , maybe even different sign than its counterpart in Eqn.23.

One can also compute the photon number correlation functions:

$$\langle n(\tau)n(0) \rangle - \langle n \rangle^2 = \frac{\omega_a\lambda_a^2}{2\omega_{-0}} \frac{2\beta}{1+\beta} e^{-(\omega_{-0}-(\Delta_1-\Delta_0)/2)\tau} \quad (25)$$

where $\langle n \rangle = \lambda_a^2$ is the photon number at the ground state. It contains the atomic energy ϵ_a minus the difference of the splittings between $n = 1$ and $n = 0$ in Fig.6 and has a spectral weight $\sim N$.

So all the parameters of the cavity systems such as the doublet splittings $\Delta_0(\alpha), \Delta_1(\alpha)$ and the atomic energy ϵ_a are encoded in the photon normal Eqn.23 and anomalous Green function Eqn.24 and photon number correlation function Eqn.25. They can be measured by photoluminescence, phase sensitive homodyne and Hanbury-Brown-Twiss (HBT) type of experiments⁴⁰ respectively.

VI. COMPARISON WITH THE RESULTS FROM THE EXACT DIAGONIZATION AND THE STRONG COUPLING EXPANSION.

When $\beta \neq 1$ in Eqn.1, it is not convenient to perform the ED in the coherent basis anymore used in¹⁵, so we did the ED in the original (Fock) basis. In the Fock space, the complete basis is $|n\rangle|j, m\rangle, n = 0, 1, 2, \dots, \infty, j = N/2, m = -j, \dots, j$ where the n is the number of photons and the $|j, m\rangle$ is the Dicke states. In performing the ED, following¹³, one has to use a truncated basis $n = 0, 1, \dots, n_c$ in the photon sector where the $n_c \sim 100$ is the maximum photon number in the artificially truncated Hilbert space. As long as the low energy levels in

Fig.7 and Fig.8 are well below $n_c\omega_a$, then the energy levels should be very close to the exact results without the truncation (namely, sending $n_c \rightarrow \infty$). However, the ED may not be precise anymore when g gets too close to the upper cutoff introduced in the ED calculation as shown in Fig.8c.

In Fig.7, we show the ED results for the energy levels for $N = 2$ at $\beta = 0.1, 0.5, 0.9, 1$. It matches precisely the theoretically predicted energy level evolutions shown in Fig.4. At $N = 2$, when $\beta < \beta_c \sim 0.6$ (which, in fact, only

The important relation Eqn.17 takes the same form as Eqn.5 in³⁹ except the absence of the extra $(-1)^l$ factor. As said at the end of Sec.IV, it is this absence of extra $(-1)^l$ which reconciles the results achieved from the two independent approaches. Eqn.16 indicates that there are infinite number of zeros due to the Berry phase interference effects in the instanton tunneling process in Fig.5. Eqn.17 indicates that the positions of the zeros are independent of n . This is indeed confirmed by the ED shown in Fig.8c for $N = 2, \beta = 0.9, l = 0, 1, 2$ where the po-

VII. EXPERIMENTAL DETECTION OF THE BERRY PHASE EFFECTS OF THE INSTANTON TUNNELING EVENTS

There have been extensive efforts to realize the Schrodinger Cat state in trapped ions⁴⁴ and superconducting qubit systems⁴⁵. Here, the Schrodinger Cats in Eqn.18 with $n = 0, 1, 2, \dots$ can be prepared in the QT regime in Fig.2a, its size can be continuously tuned from $N \sim 3 - 9$, it involves all the N number of atoms (qubits) and photons strongly coupled inside the cavity and could have important applications in quantum information processions.

With $N \sim 10^5$ atoms of ^{87}Rb inside a cavity²⁷⁻²⁹, the system is essentially in the thermodynamic limit of the Z_2 Dicke model, so the novel physical phenomena in the QT regime in Fig.2 at finite small N explored in this work are hard to observe. The experiment²⁹ first adiabatically prepared the system in one of the two bound states in Fig.3b by applying a small Z_2 symmetry breaking field, then **turn off and on** the transverse pumping laser in Fig.1a and observed the coherent switch with the frequency ω_b between the two ground states in Fig.3b by an optical heterodyne detection. As emphasized in this work, in order to observe the Berry phase interference effects, one has to move away from the Z_2 limit realized in the experiments²⁷⁻²⁹, namely, $0 < \beta < 1$. This has been realized in the recent experiment³⁶ which can tune β from 0 to 1. With the recent advances of manipulating a few atoms^{37,38}, the number of atoms can be reduced to a few to a few hundreds, then the $U(1)$ and the QT

weakly depends on N), there is always a $U(1)$ regime Fig.4b,c before the formations of bound states in the QT regime in Fig.7a,b. It is the Berry phase which leads to the parity oscillations in both regimes. However, $\beta > \beta_c$, the systems get to the formations of bound states directly in Fig.7c. It is still the Berry phase which leads to the parity oscillations in the QT regime after the formations of bound states as shown in Fig.5b. At $\beta = 1$, the Berry phase effects and the level crossings are pushed to infinity, so no parity oscillations anymore in Fig.7d.

sitions of the first $N = 2$ zeros only depend on l very weakly. So between the two zeros, at $l = 0, 1, 2, \dots$, the energy levels are either in the pattern $(e, o), (e, o), \dots$ or $(o, e), (o, e), \dots$ in Fig.4d and Fig.6b. This important result completely substantiates the results achieved from the strong coupling expansion in³⁹. The fact that the same fantastic phenomena are reached from two independent analytic approaches, then confirmed by ED indicates that the results are correct, independent of the $1/J$ expansion or strong coupling expansion we made.

regime in Fig.2, Fig.3a,b span a large parameter regimes. One can first adiabatically prepare the system in the left or right bound states in Fig.3 with $n = 0, 1, \dots$, but still **keep** the transverse pumping laser in Fig.1a, then observe by the optical heterodyne detection²⁹ the coherent oscillation probability between the two bound states:

$$P(\alpha, t) = \cos \Delta_n(\alpha)t \quad (26)$$

where the $\Delta_n(\alpha)$ is given by Eqn.17.

In circuit QED systems, there are various experimental set-ups such as charge, flux, phase qubits or qutrits, the couplings could be capacitive or inductive through Λ, V, Ξ or the Δ shape⁴⁶. Especially, continuously changing $0 < \beta < 1$ has been achieved in the recent experiment³³. As shown in²¹, by tuning the potential scattering term $\lambda_z J_z a^\dagger a / j$ and the qubit-qubit interaction term $u J_z^2 / j$, the critical coupling g_c in Fig.2 is reduced to $g_c = \sqrt{(\omega_a - \lambda_z)(\omega_b - 2u)} / (1 + \beta)$. We expect all the interesting phenomena in the $U(1)$ and QT regime in Fig.2 at a finite $N = 3 - 9$ qubits, especially the dramatic Berry phase effects in both regimes can be observed in near future experiments.

VIII. CONCLUSIONS AND DISCUSSIONS

Quantum optics differs from condensed matter physics at least in two important ways (1) the former mainly deal with finite size systems, while the latter mainly deal with thermodynamic limit (or edge states if there is a bulk

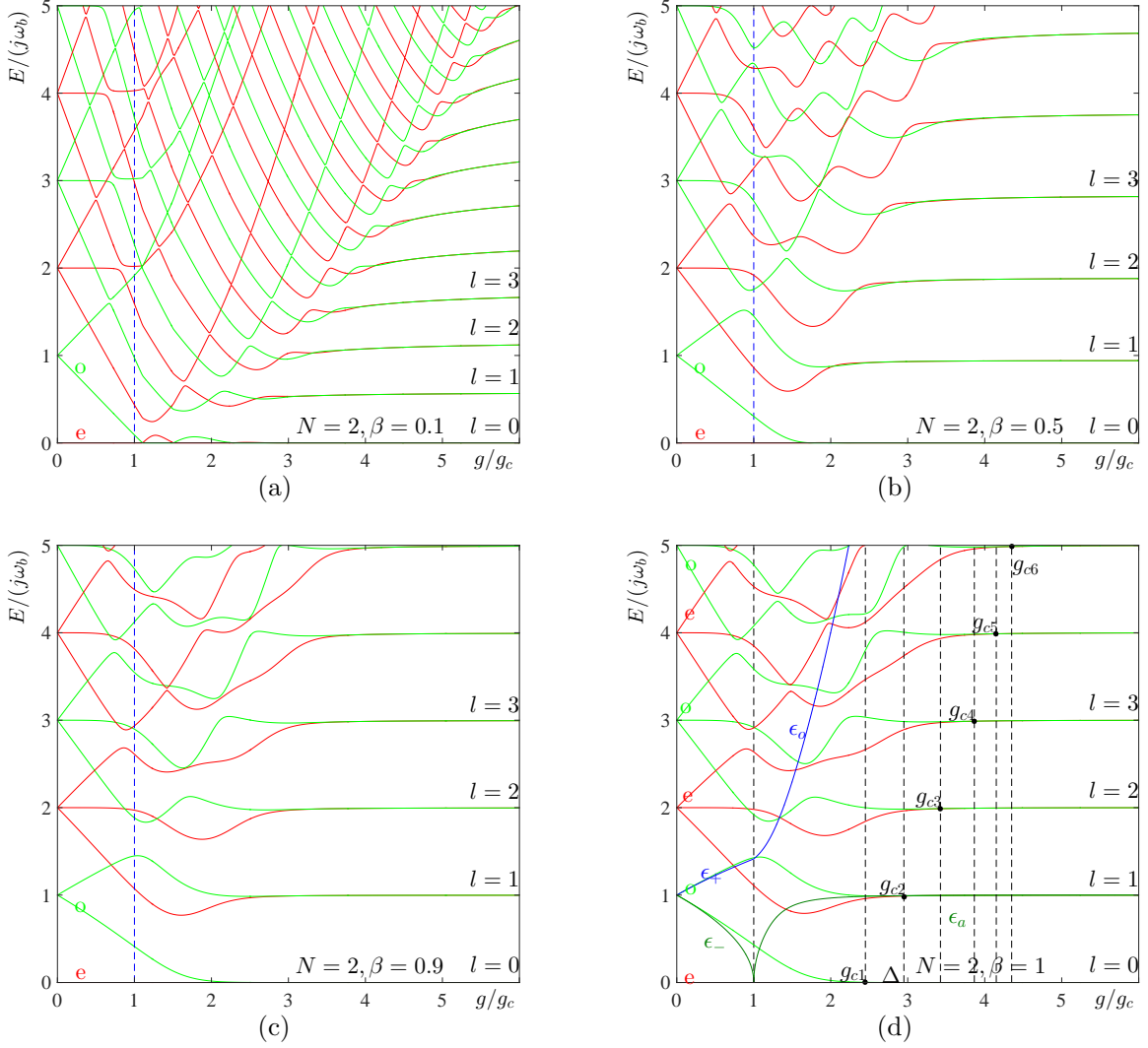


FIG. 7. ED results for the energy levels at $N = 2, \beta = 0.1, 0.5, 0.9, 1$ for (a)-(d) respectively. For simplicity, we only show $\omega_a = \omega_b$ case. The parity even (e) and odd (o) are indicated. There are none, one and two level crossing(s) in the normal regime at $l = 0, 1, 2$ respectively. (a) For $\beta = 0.1$, there are considerable ranges of the $U(1)$ regime $g_c < g < g_{c1}$ before the first bound state formation at $l = 0$, then it evolves to the QT regime where the bound states start to form at $g_{c1}, g_{c2}, g_{c3}, \dots$ (which are labeled only in (d), but could be labeled in (a)-(c) also) at $l = 0, 1, 2, \dots$ as g/g_c increases. There is a one to one correspondence to Fig.4. (b) For $\beta = 0.5$, the $U(1)$ regime becomes much smaller. (c) For $\beta = 0.9$, the $U(1)$ regime disappears. When expanding the doublets at $l = 0, 1, \dots$, as g/g_c increases, there are infinite energy level crossings leading to the oscillations of parities at the ground states at $l = 0, 1, \dots$ manifolds shown in Fig.8. As $\beta \rightarrow 1^-$, all the zeros are pushed to infinity. (d) The Z_2 limit $\beta = 1$. There are consecutive energy level mergings at $g_c < g_{c1} < g_{c1} < \dots$ which signify the bound state formations at $l = 0, 1, 2, \dots$ and the energy levels become approximately *flat*. There are no $U(1)$ regime, no level crossing between the even and odd parity pairs. The ground state pattern is $(e, o), (e, o), \dots$ at $l = 0, 1, 2, \dots$. Only the atomic energies at $l = 0, 1, 2, \dots$ are labeled. As $g/g_c \rightarrow \infty$ limit, they approach to $l\omega_a$ from below³⁹.

topological order) (2) the former mainly study pumping-decay non-equilibrium systems, while the latter mainly equilibrium systems. In this paper, we focused on the first feature. The combination of both features will be presented elsewhere⁴¹. In studying the latter, one stress " More is different " as advocated by P. W. Anderson. Here, to study the four standard quantum optics models in the former system, we take the " Few is tricky "

dual point of view²⁰⁻²² which establish the connections between the many body physics in condensed matter systems and few body problems in quantum optical systems. We introduced the generic $U(1)/Z_2$ Dicke model²¹ which incorporates all the 4 quantum optics models as its various special limits. In this paper, we investigated the new phenomena in this model at a finite N from the $1/J$ expansion which is complementary and dual to the strong

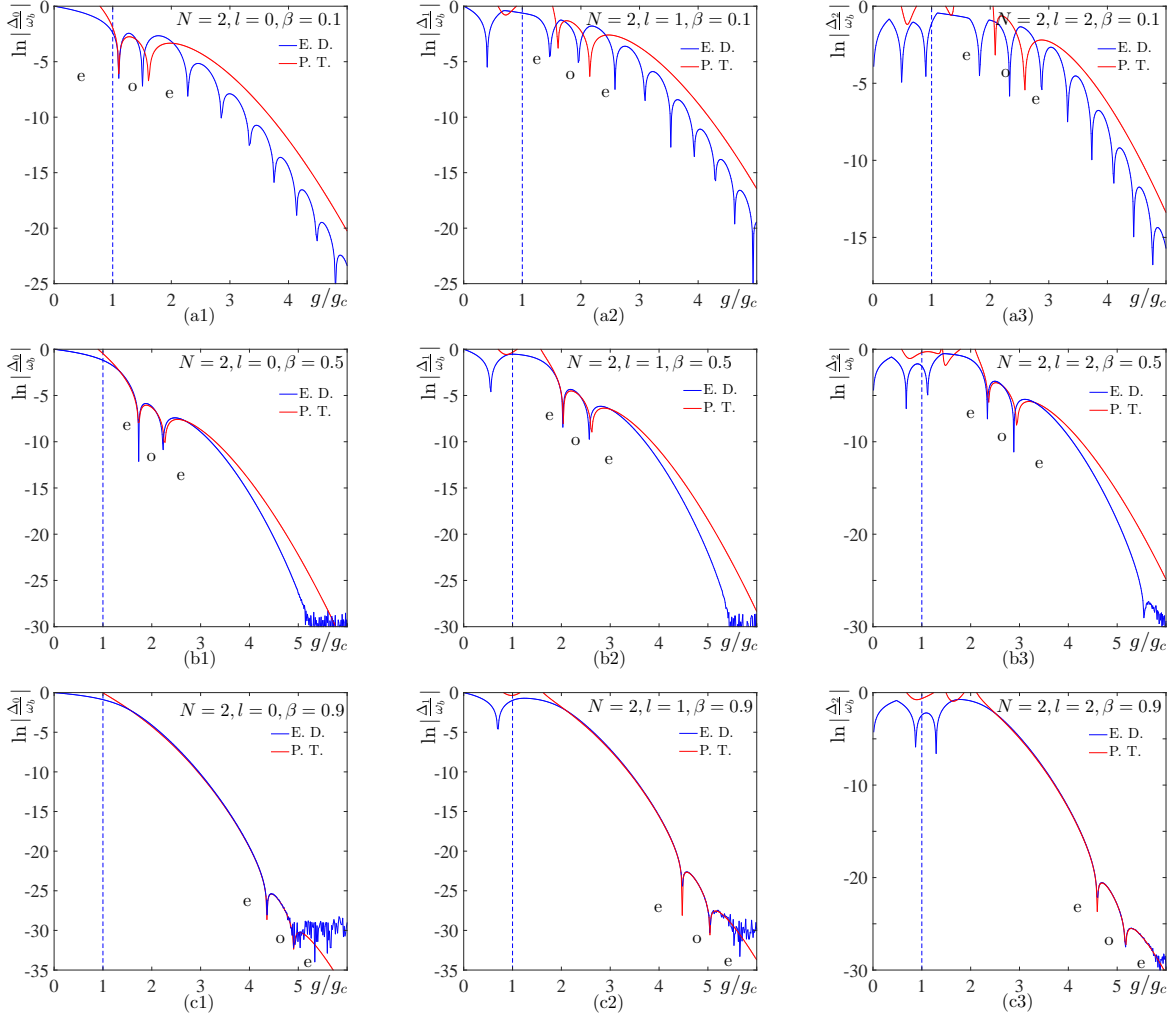


FIG. 8. Identify $U(1)$ and QT regimes in the results achieved from the strong coupling expansion and the ED³⁹. In the Log scale, the even/odd splitting Δ_l for $N = 2$ at different $\beta = 0.1, 0.5, 0.9$ in the row and at $l = 0, 1, 2$ in the column calculated by strong coupling expansion (red line) versus that by the ED (blue line)³⁹. The labels e and o are the parity of the ground states. The first even parity is in the normal regime in (a) and (b), but becomes a bound state at g_{c1} which is before the first zero in (c). The next one must be the odd parity state at $l = 0, 1, 2$. Note also the changes of the numbers in the vertical axis at the Log scale telling the splitting increases as $l = 0$ to $l = 1$, then to $l = 2$ as dictated by Eqn.8,9 for the scattering states in (a) and (b) and by Eqn.16 and 17 for the bound states in (c). There are also none, one and two level crossing(s) in the normal regime at $l = 0, 1, 2$ respectively. Eqn.16 dictates there are infinite number of zeros. The strong coupling expansion in³⁹ to N -th order only gives the first N zeros. The ED gives infinite number of zeros (but not shown here) after the first $N = 2$ zeros which can only be achieved from higher order perturbation calculations in the strong coupling expansion. (a) The strong coupling results³⁹ match well with those from ED at $l = 0$, but not too well at $l = 1, 2$ in the first $N = 2$ zeros at $\beta = 0.1$ in the $U(1)$ regime. Even so, they seem match well the envelop of the splitting at $l = 0, 1, 2$ (namely, the maximum splitting at $\alpha = 0$). This causes no concerns because the agreement is not expected in the $U(1)$ regime too close to g_c when β is small. Compare with Fig.7a, the first $N = 2$ zeros at $l = 0, 1, 2$ are due to the scattering states in the $U(1)$ regime in Fig.4b. (2) The strong coupling results³⁹ match very well with those from ED in the first $N = 2$ zeros even at $\beta = 0.5$. The other zeros are far apart from the first $N = 2$ zeros and out of the scope in the figure. Compare with Fig.7b, the first $N = 2$ zeros at $l = 0, 1, 2$ are still due to the scattering states in the narrow $U(1)$ regime in Fig.4b. Observe that the strong coupling expansion works very well and reproduces precisely the Berry phase effects in the $U(1)$ regime not too close to g_c . As shown in Fig.4b, there are shifts of zeros to the right if one follow the ground state with the odd parity. (3) The match is essentially perfect in the first $N = 2$ zeros at $\beta = 0.9$ in the QT regime. The other zeros are far apart from the first $N = 2$ zeros and out of the scope in the figure. At too strong couplings, the ED may become (noise) un-reliable due to the cutoff introduced in the ED. Compare with Fig.7c, all the zeros are well beyond $g_{c1}, g_{c2}, g_{c3}, \dots$ in Fig.7c, so the first $N = 2$ zeros are the first two bound states at $l = 0, 1, 2$ in the QT regime in Fig.2 and 4e. The $U(1)$ regime is squeezed out. Their locations are nearly independent of l as dictated by Eqn.17 for the bound states satisfying $G = \frac{g}{g_c} \frac{1}{\sqrt{N}} \gg 1$.

coupling expansion used in³⁹.

It is constructive to compare the two analytic methods. The instanton method employed in this paper which is in the spirit of path integral can map out the physical picture clearly. It starts from the $U(1)$ limit with $\beta = 0$ and animate the consecutive formation of the bound states, quantum tunneling processes subject to the Berry phase effects shown in Fig.2,3,5, the energy level evolution from the $U(1)$ to the QT regime in Fig.4. It is the Berry phase interference effects which lead to the infinite oscillations in the parity of the ground state doublets in Eqn.16 and also excited state doublets Eqn.17. It can be used to predict the zeros happen at $\alpha = \pm 1/2$ and the maximum splittings happen at $\alpha = 0$ phenomenologically, but can not used to predict where the zeros and maximum splittings happen in g/g_c . For example, it is hard to determine the behaviors of these zeros as $\beta \rightarrow 1^-$ limit. Only when taking the results achieved from the strong coupling expansion from the $\beta = 1 Z_2$ limit, one can see that all the zeros are pushed into infinity in the Z_2 limit. However, we need to evaluate the photon correlations functions Eqn.23, 24 and 25 separately in the $U(1)$ regime (Fig.6a) by the perturbation theory and in the QT regime (Fig.6b) in an intuitive and phenomenological way. The strong coupling expansion employed in³⁹ which is in the spirit of canonical quantization can not distinguish the differences between the scattering states and the bound states, therefore not the physical process of the bound state formation in Fig.2,3,5. It starts from the Z_2 limit with $\beta = 1$. The Berry phase effects are only implicitly embedded in the expansion in term of the anisotropic parameter away from the Z_2 limit $\beta \neq 1$. So the physical picture is less clear. However, it can be used to evaluate the first N zeros very precisely when compared with the ED in Fig.7 and Fig.8. It can also be used to calculate all the photon correlation functions in both the QT and $U(1)$ regimes systematically and in a unified scheme. So the two analytical methods are complementary and dual to each other. Their combination leads to rather complete understandings of both physical mechanisms and quantitative values of all the experimental measurable quantities in the QT regimes and the $U(1)$ regime not too close to the QCP at $N = \infty$ in Fig.2 and 4.

At the $U(1)$ limit $\beta = 0$, there are infinite level crossings due to the Berry phase effects at a finite N (Fig.4a) as presented in²⁰⁻²². Turning on a small β will only lead to level repulsions between the same parity states, the Berry phase still leads to the level crossings between the even and odd state, therefore the alternating parities on the ground state and also all the doublets at $|m| = 1, \dots, P$ in the $U(1)$ regime (Fig.4b). When β gets bigger, the system evolves into the QT regime where the Berry phase continue to play a crucial role leading to interference between different instanton tunneling events (Fig.4c and d). As β gets close to 1, the $U(1)$ regimes disappears, the normal state directly gets to the QT regime, the Berry phase effects show up after the formations of

all the bound states. At the Z_2 limit $\beta = 1$, $\lambda = 0$, the Berry phase effects are pushed into infinity, so there is no level crossings between opposite parities anymore in Fig.7d, the energy levels statistics at a given parity sector satisfy the Wigner-Dyson distribution in the superradiant regime¹³. However, at any $\beta < 1$ in Eqn.1, as shown in³⁹, it is the extra term $\lambda(a^\dagger - a)iJ_y$ which introduces frustrations, therefore Berry phase effects into the $Z_2/U(1)$ Dicke model. They leads to infinite level crossings with alternating even and odd parity in the ground state and all the doublets at $l > 1$ (Fig.4d). Combining the physical picture from β small achieved from $U(1)$ limit by instanton method in this paper to large $\beta \sim 1$ achieved from Z_2 limit by the strong coupling expansion method in³⁹, we conclude that it is the Berry phase effects which lead to the level crossings at any $0 \leq \beta < 1$ except at the Z_2 limit $\beta = 1$. From Fig.4, we expect that the level statistics at a given parity sector still satisfies the Poisson statistics in the normal regime, the Wigner-Dyson distribution in the QT regime, but it remains interesting to see how it changes in the $U(1)$ regime in Fig.2. It was shown in Ref.⁴⁷ that it is Berry phase effects in the instanton tunneling events in the 2+1 compact QED which leads to the Valence bond order in 2d quantum Anti-ferromagnet. Here we showed that it is Berry phase effects in the 0 + 1 dimensional instanton tunneling events in the compact phase of photons which leads to the infinite level crossing with alternating parity in the ground and low energy excited states (Fig.4,7).

There are some illuminating duality in both the Hamiltonian and the quantum numbers characterizing the energy spectrum of the $U(1)/Z_2$ Dicke model. In the present paper, we start from the Hamiltonian in its $U(1)/Z_2$ representation Eqn.1 and use its complete eigenstates $|l\rangle_m|m\rangle$ when β is not too large (namely near the $U(1)$ limit). In the $U(1)$ crossover regime in Fig.2 and 4, the Landau level index $l = 0, 1, \dots, N$ ($N + 1$ Landau levels) denotes the high energy Higgs type of excitation, the magnetic number $m = -P, -P + 1, \dots$ (no upper bounds) denotes the low energy pseudo-Goldstone mode²¹. However, in the strong coupling expansion used in³⁹, we start from the Hamiltonian in its dual $Z_2/U(1)$ representation and use its complete eigenstates $|l\rangle_m|j, m\rangle$ when $1 - \beta$ is not too large (namely near the Z_2 limit). In the QT regime in Fig.2 and 4, the Landau level index $l = 0, 1, \dots$ (no upper bounds) denotes the low energy atomic excitation, the magnetic number $m = -j, -j + 1, \dots, j$ (also $2j + 1 = N + 1$) denotes the high energy optical mode. So the Landau level index and the magnetic number exchanges their roles from the $U(1)$ to the QT regime. The crossover between the two basis is precisely described in Fig.4. Of course, when β gets too close to 1, the $U(1)$ regime disappears and so does the duality relations.

Acknowledgements

J. Ye thank Yu Chen for his participation and Prof. Guangshan Tian for encouragements in the very early stage of the project. We thank Han Pu and Lin Tian for

helpful discussions. Y.Y and JY are supported by NSF-DMR-1161497, NSFC-11174210. W.M. Liu is supported by NSFC under Grants No. 10934010 and No. 60978019, the NKBRSC under Grants No. 2012CB821300. CLZ's work has been supported by National Keystone Ba-

sic Research Program (973 Program) under Grant No. 2007CB310408, No. 2006CB302901 and by the Funding Project for Academic Human Resources Development in Institutions of Higher Learning Under the Jurisdiction of Beijing Municipality.

-
- ¹ D. F. Walls and G. J. Milburn, *Quantum Optics*, Springer-Verlag, 1994.
- ² M. O. Scully and M. S. Zubairy, *Quantum Optics*, Cambridge University press, 1997
- ³ I.I. Rabi, *Phys. Rev.* 49, 324 (1936); 51, 652 (1937).
- ⁴ E. T. Jaynes and F. W. Cummings, *Proc. IEEE* 51, 89 (1963).
- ⁵ R.H. Dicke, *Phys. Rev.* 93, 99 (1954)
- ⁶ M. Tavis and F.W. Cummings, 170, 379 (1968).
- ⁷ A. Auerbach, *Interacting electrons and quantum magnetism*, (Springer Science & Business Media, 1994).
- ⁸ S. Sachdev, *Quantum Phase transitions*, (2nd edition, Cambridge University Press, 2011).
- ⁹ K. Hepp and E. H. Lieb, *Anns. Phys. (N. Y.)*, 76, 360 (1973); Y. K. Wang and F. T. Hioe, *Phys. Rev. A*, 7, 831 (1973).
- ¹⁰ V. N. Popov and S. A. Fedotov, *Soviet Physics JETP*, 67, 535 (1988); V. N. Popov and V. S. Yarunin, *Collective Effects in Quantum Statistics of Radiation and Matter* (Kluwer Academic, Dordrecht,1988).
- ¹¹ P. R. Eastham and P. B. Littlewood, *Phys. Rev. B* 64, 235101 (2001).
- ¹² V. Buzek, M. Orszag and M. Roko, *Phys. Rev. Lett.* 94, 163601 (2005).
- ¹³ C. Emary and T. Brandes, *Phys. Rev. Lett.* 90, 044101 (2003); *Phys. Rev. E* 67, 066203 (2003). N. Lambert, C. Emary, and T. Brandes, *Phys. Rev. Lett.* 92, 073602 (2004).
- ¹⁴ J. Vidal and S. Dusuel, *Finite-size scaling exponents in the Dicke model*, *Europhys. Lett.* 74, 817 (2006).
- ¹⁵ Qing-Hu Chen, Yu-Yu Zhang, Tao Liu and Ke-Lin Wang, *Numerically exact solution to the finite-size Dicke model*, *Phys. Rev. A* 78, 051801(R) (2008).
- ¹⁶ Note that For the general $U(1)/Z_2$ Dicke model Eqn.1 with $0 < \beta < 1$, the normal to the superradiant transitions at $N = \infty$ share the same universality class as the Z_2 limit at $\beta = 1$, so only the coefficient c depends on β . As shown here, the dramatic qualitative differences due to $\beta \neq 1$ show up only away from the QCP in the $U(1)$ and QT regime in Fig.2. It is the purpose of this manuscript to explore the new phenomena in the $U(1)$ and QT regime at a general $0 < \beta < 1$ at a finite N .
- ¹⁷ R. Botet, R. Jullien, and P. Pfeuty, *Size Scaling for Infinitely Coordinated Systems*, *Phys. Rev. Lett.* 49, 478 (1982); *Large-size critical behavior of infinitely coordinated systems*, *Phys. Rec. B*, 28, 3955 (1983).
- ¹⁸ The $U(1)$ Dicke (Tavis-Cummings) model is integrable at any finite N , so, in the " face " value, the system's eigen-energy spectra could be "exactly" solvable by Bethe Ansatz like methods. For example, see N.M. Bogoliubov, R.K. Bullough, and J. Timonen, *Exact solution of generalized Tavis-Cummings models in quantum optics*, *J. Phys. A: Math. Gen.* 29 6305 (1996). However, so far, the Bethe Ansatz like solutions stay at very "formal" level from which it is even not able to get the system's eigen-energy analytically, let alone to extract any underlying physics. Furthermore, it is well known the Bethe Ansatz method is not able to get any dynamic correlation functions.
- ¹⁹ D. Braak, *Phys. Rev. Lett.* 107, 100401 (2011). It is difficult to even derive $\langle n_{ph} \rangle \sim cN^{1/3}$ scaling near the QCP and also any interesting phenomenon achieved in the present paper in the $U(1)$ and QT regime in Fig.2 from the formally exact solution even at the simplest case $N = 1, \beta = 1$. It would be impossible to calculate the dynamic photon correlation functions.
- ²⁰ Jinwu Ye and CunLin Zhang, *Super-radiance, Photon condensation and its phase diffusion*, *Phys. Rev. A* 84, 023840 (2011).
- ²¹ Yu Yi-Xiang, Jinwu Ye and W.M. Liu, *Scientific Reports* 3, 3476 (2013).
- ²² Yu Yi-Xiang, Jinwu Ye, W.M. Liu and CunLin Zhang, *arXiv:1506.06382*.
- ²³ J. Ye and S. Sachdev, *Phys. Rev. B* 44, 10173 (1991); J. Ye, S. Sachdev and N. Read, *Phys. Rev. Lett.* 70, 4011 (1993); A. Chubukov, S. Sachdev and J. Ye ; *Phys. Rev. B* 49, 11919 (1994); Jinwu Ye and S. Sachdev; *Phys. Rev. Lett.* 80, 5409 (1998); Jinwu Ye, *Phys. Rev. B* 60, 8290 (1999).
- ²⁴ For strong coupling expansions and $1/S$ spin wave expansion in spin-orbit coupled lattice systems, see Fadi Sun, Jinwu Ye, Wu-Ming Liu, *Phys. Rev. A* 92, 043609 (2015); *arXiv:1502.05338*.
- ²⁵ Ferdinand Brennecke, Tobias Donner, Stephan Ritter, Thomas Bourdel, Michael Khl, Tilman Esslinger, *Cavity QED with a Bose-Einstein condensate*, *Nature* 450, 268 - 271 (08 Nov 2007).
- ²⁶ Yves Colombe, Tilo Steinmetz, Guilhem Dubois, Felix Linke, David Hunger, Jakob Reichel, *Strong atom-field coupling for Bose-Einstein condensates in an optical cavity on a chip*, *Nature* 450, 272 - 276 (08 Nov 2007).
- ²⁷ A. T. Black, H. W. Chan and V. Vuletic, *Observation of Collective Friction Forces due to Spatial Self-Organization of Atoms: From Rayleigh to Bragg Scattering*, *Phys. Rev. Lett.* 91, 203001(2003).
- ²⁸ K. Baumann, *et.al*, *Dicke quantum phase transition with a superfluid gas in an optical cavity*, *Nature* 464, 1301-1306 (2010);
- ²⁹ K. Baumann, R. Mottl, F. Brennecke, and T. Esslinger, *Exploring Symmetry Breaking at the Dicke Quantum Phase Transition*, *Phys. Rev. Lett.* 107, 140402 (2011).
- ³⁰ A. Wallraff, *et.al*, *Strong coupling of a single photon to superconducting qubit using circuit quantum electrodynamics*, *Nature* 431, 162-167 (2004)
- ³¹ G. Gunter, A. A. Anappara, J. Hees, A. Sell, G. Biasiol, L. Sorba, S. De Liberato, C. Ciuti, A. Tredicucci, A. Leitenstorfer, R. Huber, *Sub-cycle switch-on of ultra-strong light-matter interaction*, *NATURE*, Vol 458, 178, 12 March 2009.
- ³² Aji A. Anappara, Simone De Liberato, Alessandro

- Tredicucci, Cristiano Ciuti, Giorgio Biasiol, Lucia Sorba, and Fabio Beltram, Signatures of the ultrastrong light-matter coupling regime, *Phys. Rev. B* 79, 201303(R) (2009).
- ³³ T. Niemczyk, *et.al*, Circuit quantum electrodynamics in the ultrastrong-coupling regime, *Nature Physics* 6, 772C776(2010).
- ³⁴ Reithmaier, J. P, *et.al*, Strong coupling in a single quantum dot-semiconductor micro-cavity system, *Nature* 432, 197-200 (2004). Yoshie, T. *et al*, Vacuum Rabi splitting with a single quantum dot in a photonic crystal nanocavity, *Nature* 432, 200-203 (2004). K. Hennessy, A. Badolato, M. Winger, D. Gerace, M. Atatüre, *et al*, Quantum nature of a strongly coupled single quantum dot-cavity system, *Nature* 445, 896-899 (22 February 2007).
- ³⁵ F. Dimer, B. Estienne, A. S. Parkins, and H. J. Carmichael, *Phys. Rev. A*, 75, 013804, 2007
- ³⁶ Markus P. Baden, Kyle J. Arnold, Arne L. Grimsmo, Scott Parkins, and Murray D. Barrett, Realization of the Dicke Model Using Cavity-Assisted Raman Transitions, *Phys. Rev. Lett.* 113, 020408 C Published 10 July 2014.
- ³⁷ W. S. Bakr, *et.al*, Probing the Superfluid-to-Mott Insulator Transition at the Single-Atom Level, *Science* 30 July 2010: 547-550.
- ³⁸ F. Serwane, *et.al*, Deterministic Preparation of a Tunable Few-Fermion System, *Science* 15 April 2011: 336-338.
- ³⁹ Yu Yi-Xiang, Jinwu Ye and CunLin Zhang, Parity oscillations and photon correlation functions in the $Z_2/U(1)$ Dicke model at a finite number of atoms or qubits, Preprint.
- ⁴⁰ Jinwu Ye, T. Shi and Longhua Jiang, *Phys. Rev. Lett.* 103, 177401 (2009); T. Shi, Longhua Jiang and Jinwu Ye, *Phys. Rev. B* 81, 235402 (2010); Jinwu Ye, Fadi Sun, Yi-Xiang Yu and Wuming Liu, *Ann. Phys.* 329, 51C72 (2013).
- ⁴¹ Yu Yi-Xiang, Jinwu Ye and CunLin Zhang, unpublished.
- ⁴² S. Coleman, *Aspects of Symmetry*, Cambridge University Press, 1985, A. M. Polyakov, *Gauge Fields and Strings*, Harwood Academic Publishers, 1987; R. Rajaraman, *Solitons and Instantons*, North-Holland Publishing Company, 1982
- ⁴³ U. Weiss and W. Haffner, *Phys. Rev. D* 27, 2916 (1983).
- ⁴⁴ C. Monroe, D. M. Meekhof, B. E. King, and D. J. Wineland, A Schrodinger Cat Superposition State of an Atom, *Science* 24 May 1996: 1131-1136; D. Leibfried, E. Knill, S. Seidelin, J. Britton, R. B. Blakestad, J. Chiaverini, D. B. Hume, W. M. Itano, J. D. Jost, C. Langer, et al, I. Creation of a six-atom Schrödinger cat state, *Nature* 438, 639-642 (1 December 2005).
- ⁴⁵ Jonathan R. Friedman, Vijay Patel, W. Chen, S. K. Tolpygo, J. E. Lukens, I. Quantum superposition of distinct macroscopic states, *Nature* 406, 43-46 (6 July 2000). Caspar H. van der Wal, A. C. J. ter Haar, F. K. Wilhelm, R. N. Schouten, C. J. P. M. Harmans, T. P. Orlando, Seth Lloyd, and J. E. Mooij, Quantum Superposition of Macroscopic Persistent-Current States, *Science* 27 October 2000: 773-777.
- ⁴⁶ For reviews, see J. Q. You, Franco Nori, Atomic physics and quantum optics using superconducting circuits, *Nature* 474, 589 (2011). Steven M. Girvin, Superconducting Qubits and Circuits: Artificial Atoms Coupled to Microwave Photons, Lectures delivered at Ecole d'Ete Les Houches, July 2011 To be published by Oxford University Press.
- ⁴⁷ N. Read and S. Sachdev, *Nucl. Phys. B* 316, 609 (1989); *Phys. Rev. Lett.* 62, 1694 (1989); *Phys. Rev. B* 42, 4568 (1990), *Phys. Rev. Lett.* 66, 1773 (1991). G. Murthy and S. Sachdev, *Nucl. Phys. B* 344, 557 (1990).